

Modelling The Behaviour Of Sand Under Strain-Controlled Loading BY The Finite Element Method

Omar al-Farouk S. al-Damluji* **Mohammed Yousif Fattah****

Yousif J. al-Shakarchi*

Received on: 23/1/2007

Accepted on: 7/6/2007

Abstract:

Strain-controlled tests are conventional in soil mechanics laboratories. It is intended in this paper to simulate both triaxial and simple shear tests theoretically by using the finite element method. The solution of the non-linear equations is obtained by several iterations. The Newton-Raphson with tangent stiffness method in which the stiffness matrices are tangents is adopted. The model used in this paper is the ALTERNAT model which forms the major component of a double hardening model for the mechanical behaviour of sand under alternating loading.

The finite element method is used in simulating the behaviour of round uniform quartz sand under monotonic drained loading with constant mean stress and cyclic constant volume loading (undrained). The monotonic test was conducted with constant mean stress, where the specimen was compressed in one direction and extended in other directions while the mean stress (the average of the principal stresses) is kept constant and equal to 137 kPa. It is noticed that the peak stress is occurring at very small strain (0.122). The stress-strain behaviour may be attributed to the particle roundness and grain size uniformity.

In the cyclic tests, the specimen is sheared by cycling the shear strain while the volume was kept constant. By doing this, an undrained strain-controlled cyclic test similar to that typically done in many laboratories is numerically simulated.

It was found that the mean stress during shearing is higher than the initial consolidation pressure. This implies that only negative pore pressures occur in the first two cycles. A careful study shows that there exists an effective stress ratio line or zero-dilatancy line in both compression and extension regions, beyond which the specimen dilates.

Keywords: Strain-Controlled, Sand, Finite Elements, Cyclic, ALTERNAT Model.

* Civil Eng. Dept., College of Eng., Univ. of Baghdad.

** Building and Construction Eng. Dept., Univ of Technology.

الخلاصة:

تعتبر فحوص الانفعال المسيطر عليه شائعة في مختبرات ميكانيك التربة. يهدف هذا البحث إلى تمثيل كل من فحص الانضغاط ثلاثي المحاور و فحص القص البسيط نظريا بطريقة العناصر المحددة. يتم حل المعادلات اللاخطية بعدة محاولات حيث تعتمد طريقة مصفوفة الصلادة المماسية أو مصفوفة نيوتن-رافسون. إن النموذج المستعمل في هذا البحث هو لنموذج ALTERNAT الذي يشكل المركبة الرئيسية لانموذج ثنائي التصلب يستعمل لتمثيل السلوك الميكانيكي للرمال تحت تأثير أحمال متغيرة. أستعملت طريقة العناصر المحددة في تمثيل سلوك رمل مستدير الحبيبات منتظم من الكوارتز معرض إلى حمل مبزول أحادي تحت تأثير معدل إجهاد ثابت و حمل دوري غير مبزول تحت تأثير حجم ثابت.

أجري الفحص الأحادي بتثبيت معدل الإجهاد حيث يتم ضغط النموذج من اتجاه معين و استطالته من الاتجاهين الآخرين بينما يبقى معدل الإجهادات الرئيسية ثابتا و مساويا إلى ١٣٧ كيلوباسكال. و قد لوحظ أن إجهاد القمة يحدث عند انفعال صغير جدا (٠,١٢٢)، و يمكن أن تعزى علاقة الإجهاد-الانفعال هذه إلى استدارة الحبيبات و انتظام أحجامها. أما في الفحوص الدورية فيتم قص النموذج بتكرار انفعال القص مع إبقاء الحجم ثابتا. و بهذه العملية يتم تمثيل فحص دوري غير مبزول فيه الانفعال مسيطر عليه بحالة مماثلة لما يحدث في المختبر. و قد وجد أن معدل الإجهاد خلال القص يكون أعلى من ضغط الانضمام الأولي، و هذا يعني أنه يحدث ضغط ماء سالب في الدورتين الأوليتين. و عند ملاحظة النتائج بدقة يتبين وجود خط يمثل نسبة إجهاد مؤثر أو ما يسمى بخط التمدد الصفري (Zero Dilatancy Line) في كل من منطقتي الضغط و الشد، و يبدأ النموذج بالتمدد خارج هذين الخطين.

Introduction:

Strain-controlled tests are conventional in soil mechanics laboratories, for example triaxial test and direct shear test. In the following sections, this type of control is modelled through the finite element method.

The model described in this paper forms the major component of a double hardening model for the mechanical behaviour of sand under alternating loading. The model was developed by Molenkamp (1987) at Delft Geotechnics. In Fig. (1), the yield surfaces of both plastic models, namely the

“compressive” model and the “deviatoric” model are shown in the stress space of the isotropic stress, s , and the deviatoric stress, t .

The Yield Surface for the Deviatoric Model:

For the continuum model of a uniform stack of rigid discs, a kind of kinematic yield surfaces was found, (Fig. 2) in which the relevant measure of stress appeared to be a shear stress level (Molenkamp, 1980). For the present kinematic model, a similar measure of a relevant stress is introduced, namely the shear stress level which is defined by:

$$\frac{t_{ij}}{\frac{I_1}{3}} = \frac{s_{ij} - \frac{I_1}{3}d_{ij}}{\frac{I_1}{3}} \quad (1)$$

in which:

- t_{ij} = deviatoric stress,
- σ_{ij} = stress tensor,
- $I_1 = \sigma_{ij} \delta_{ij} = \sigma_{ii}$ = first stress invariant,
- δ_{ij} = Kronecker's delta.

This relevant measure of stress in Eq. (1) is dimensionless.

For the tensor of anisotropy, also a dimensionless deviatoric tensor, ξ , is introduced, thus $\xi_{ij} \xi_{ij} = 0$. The relevant measure of the pseudo shear stress level becomes:

$$\frac{X_{ij}}{\frac{I_1}{3}} = \frac{t_{ij}}{\frac{I_1}{3}} - x_i \quad (2)$$

in which: X_{ij} = deviatoric pseudo stress tensor.

The expression chosen for the yield surface F^d should reduce to a generally accepted expression for monotonic loading when $\xi_{ij} = 0$. The expression as introduced by Lade and Duncan (1975) is used:

$$F^d = \frac{I_1^3}{I_3} - 27 - f^d(x) = 0 \quad (3)$$

in which:

$$f^d = \frac{I_1^3}{I_3} - 27 \quad \text{measure of}$$

the shear stress level, constant at a kinematic yield surface for a definite value of the hardening parameter, χ , as shown in Fig. (2).

I_3 is the third stress invariant.

The Plastic Potential for the Deviatoric Model:

In a plastic material model, the plastic potential describes the ratio of the Eulerian strain rates. For simplicity, it is assumed that the ratios of the plastic Eulerian strain rates can be described in the following way:

$$\frac{\dot{\epsilon}_{ij}^d}{\dot{\epsilon}} = \frac{\dot{\epsilon}_{ij}^d}{\dot{\epsilon}} \frac{\dot{\epsilon}}{\dot{\epsilon}} + \frac{\dot{\epsilon}_{ij}^{dd}}{\dot{\epsilon}} = \frac{\dot{\epsilon}_{ij}^{dd}}{\dot{\epsilon}} \quad (4)$$

in which:

$$\frac{\dot{\epsilon}_{ij}^{dd}}{\dot{\epsilon}} x_{ij} = 0 \quad (5)$$

= deviatoric tensor

and

$$\frac{\dot{\epsilon}_{kl}^{dd}}{\dot{\epsilon}} \frac{\dot{\epsilon}_{kl}^{dd}}{\dot{\epsilon}} = 1 \quad (6)$$

α is the *angle of noncoaxiality* which is the angle between the principal directions of stress and the Eulerian strain rates.

Like the yield surface, the deviatoric component of the plastic potential G^{dd} is based on the failure surface of Lade and Duncan (1975), namely:

$$F^* = \frac{I_1^{3*}}{I_3^*} - 27 - f^{d*} = 0 \tag{7}$$

in which: I_1^* , I_3^* are the first and third invariants of the pseudo stress T_{ij}^* . The pseudo stress T_{ij}^* has the same isotropic component as the pseudo stress $T_{ij} = \sigma_{ij} - I_1/3$ as used for the yield surface but a smaller deviatoric part.

Details of the functions and the ALTERNAT model are given by Molenkamp (1987) and Fattah (1999).

Stress Dilatancy:

Molenkamp (1980) elaborated the stress dilatancy theory for triaxial compression and triaxial extension tests. For loading towards failure in triaxial compression, it was found that:

$$\frac{\dot{V}}{\dot{g}} = \frac{-\sqrt{2}(1-K) - (2+K)\frac{t}{s}}{(1+2K) + \sqrt{2}(1-K)\frac{t}{s}} \tag{8}$$

in which:

$$K = \tan^2\left(45 + \frac{f_o}{2}\right)$$

V = volumetric strain,

γ = deviatoric strain, and

ϕ_o = the interparticle friction angle.

It is assumed that, (Molenkamp, 1980):

$$f_o = f_{cv} - (f_{cv} - f_m) \exp\left\{-\frac{s}{Pa \cdot S_{cv}}\right\} \tag{9}$$

in which:

ϕ_μ = interparticle friction angle at very low isotropic stress, s ,

ϕ_{cv} = interparticle friction angle at very high isotropic stress,

S_{cv} = parameter describing the rate by which ϕ_o changes from ϕ_μ to ϕ_{cv} with increasing isotropic stress level (s/Pa), (see Fig. 3),

s = isotropic stress, and

Pa = atmospheric pressure.

For loading towards failure in triaxial extension, it was found that:

$$\frac{\dot{V}}{\dot{g}} = \frac{\sqrt{2}(1-K) - (1+2K)\frac{t}{s}}{(2+K) - \sqrt{2}(1-K)\frac{t}{s}} \quad (10)$$

Extension of the ALTERNAT Model:

In the numerical simulation of the behaviour of frictional materials under alternating loading, the small errors in the calculation of each individual increment may accumulate partly in subsequent increments. This property of numerical models is known as "*numerical drift*".

Molenkamp (1990) described an algorithm to minimize eventual numerical drift due to cyclic loading. One aspect involves the automatic control of the magnitude of the applied subincrements of stress and strain. The other aspect concerns a corrective procedure to keep the relevant stresses on the corresponding yield surfaces. Consequently, eventual errors in the plastic

deformation will not accumulate.

A combination of the parameters of the previous version of the ALTERNAT model (1987) and the present one will be used in this paper.

The range of validity of the ALTERNAT model had been extended by Molenkamp (1990) from small strain to large strain deformation. To this end, also the concept of the critical state had been applied. Details of the application are given by Fattah (1999).

Determination of the ALTERNAT Model Parameters:

For the determination of the parameters of the ALTERNAT model described in the previous sections, special types of triaxial tests are required, e.g., drained triaxial tests with monotonically increasing or decreasing axial strain and constant isotropic stress. These tests are not easy to be conducted in soil mechanics laboratories. It is intended here to choose a simple theoretical model to get the required stress - strain relationships for the

determination of ALTERNAT model parameters.

Of many theoretical models available to predict the overall response of sands, the "endochronic model" was chosen for this task. This model treats the sand as a non-linear elasticplastic material. Furthermore, the theory assumes inelastic changes to be caused only by the rearrangement of grains.

In this paper, the original version of the endochronic theory adopted by Bazant and Krizek (1976) is used because of its numerical simplicity. This version was limited to drained conditions and will be extended to include undrained conditions. Fattah (1999) gave detailed investigation about using the endochronic model in determining ALTERNAT model parameters. For the description of the ALTERNAT model parameters, see Molenkamp (1987 and 1990).

Applications:

Ng and Dobry (1994) made experimental and theoretical investigation on granular specimens composed of uniform spheres.

The discrete element method (DEM) was used in simulating round uniform quartz sand under monotonic drained loading with constant mean stress and cyclic constant volume loading (undrained).

In the DEM, the interaction between particles is considered as a transient problem with states of equilibrium developing when the internal forces balance. The equilibrium contact forces and displacements are found in a stressed assembly of particles through a series of calculations tracing the movements of each individual grain, (Cundal and Strack, 1979).

A typical 2-dimensional specimen used by Ng and Dobry (1994) is shown in Fig. (4). The porosity was calculated as the ratio between the pore area of the plane where the spheres' centers lie and the box dimensions. In general 3-dimensional specimens, the porosity was defined as $n = (1 - \sum \text{volume of spheres}) / \text{volume of box}$.

Two simulated granular specimens composed of spheres were used in this study (specimens B and C). All

particles were assigned the properties of quartz: shear modulus, $G = 28.957$ MPa, Poisson's ratio, $\nu = 0.15$, and the friction coefficient $\mu_s = \tan \phi_o = 0.5$ where ϕ_o is the interparticle friction angle.

The specimens are described in Table (1) in which the third and fourth columns show the total number of spherical particles N used in each specimen, as well as the ratios $R_1/R_2/R_3$ of three different particle sizes with $N_1/N_2/N_3$ which are the numbers of particles having these sizes.

In all cases, $N = N_1+N_2+N_3$ and all the specimens were isotropically consolidated to $\sigma_c = 137$ kPa prior to monotonic and cyclic loading.

Strain-Controlled Loading for the Kinematic Hardening Model:

It is intended in this paper to simulate both triaxial and simple shear tests. Therefore, the principle of the computations for the strain-controlled loading is discussed in this section. The calculations for the strain-controlled loading had been collected in the

program STRINS (Molenkamp, 1987).

First a choice is met; it concerns the question whether in the previous increment, viscous flow (no cracking) has occurred. If so, the stress due to viscous flow is calculated by:

$$s_{ij} = 2n \frac{\dot{\epsilon}_{ij}}{\dot{\epsilon}} - d_{ij} \frac{\dot{\epsilon}_{kl} d_{kl}}{3} \quad (11)$$

in which ν is the viscosity. In the program, the arbitrary parameter VISC is used, which is related to the viscosity by:

$$n = VISC * Pa \quad (12)$$

in which Pa is the atmospheric pressure.

If previously no viscous flow (or cracking) has occurred, then the following actions are performed. First the effect of cohesion c is taken into account by adapting the normal stresses:

$$s_{cii} = s_{ii} + \frac{c}{\tan f_{cv}} \quad (13)$$

Also the apparent isotropic stress at liquefaction or cracking P_{liq} is calculated, namely:

$$P_{liq} = \frac{c}{\tan f_{cv}} - P_{tens}$$

in which P_{tens} = strength in isotropic tension in case of cohesion.

In case of liquefaction without cohesion, for P_{tens} a small pressure is used, namely:

$$P_{tens} = - Pa * 10^{-5} \tag{14}$$

Later in the sequence of actions, the liquefaction or cracking is assumed to begin if:

$$\frac{S_{c11} + S_{c22} + S_{c33}}{3} < P_{liq} \tag{15}$$

The stress increment in case of elastic behaviour needed for the later evaluation of the type of loading is derived in the co-rotational frame of reference. The incremental rotation for the eventual back transform of the computed stress is determined. The strain increment is provided in the fixed frame of reference. It is converted to the co-rotational frame of reference. The determination of the type of behaviour is based on a number of criteria.

First of all, the previous behaviour is continued if it was

viscous flow. The stress increments and new stresses are then determined assuming purely elastic behaviour. The elastic strain increment is used to determine the type of loading. For this purpose, several criteria for stress reversals are available. For more explanations see Fattah (1999).

Implementation of the Kinematic Hardening Model in Finite Element Discretization:

In this section, a physical problem with its finite element approximation will be treated. The attention will be focused on the static problem.

Equilibrium Problem and its Finite Element Formulation:

The stress tensor, σ_{ij} , is required to satisfy the equilibrium equation:

$$S_{ij,i} + F_j = 0 \tag{16}$$

in the region v.

The finite element approximation can be written as:

$$\int_{\tilde{v}} \tilde{B}^T \tilde{S} \tilde{dv} + \tilde{f} = 0$$

where \tilde{s} is a function of the displacement; i.e., the displacements at the nodes of the elements.

The practical situation is usually starting from an equilibrium state stress \tilde{s}^0 , and tractions \tilde{f}^0 , thus some changes are enforced such that either the displacement or the surface traction are adapted. Schematically one may write:

$$\partial \tilde{B}^T \tilde{s}^0 dv + \tilde{f}^0 = 0 \quad (17)$$

$$\tilde{s} = \tilde{s}^0 + D \tilde{s} \quad (18)$$

$$\tilde{f} = \tilde{f}^0 + D \tilde{f} \quad (19)$$

then:
$$\partial \tilde{B}^T D \tilde{s} + D \tilde{f} = 0 \quad (20)$$

For a linear elastic model, the stress is given by:

$$D \tilde{s} = D D \tilde{s} \quad (21)$$

and

$$D \tilde{e} = B D U \quad (22)$$

where: D = the stress-strain matrix.

B = the strain-nodal displacement matrix.

The substitution of equations (21) and (22) results in:

$$\partial \tilde{B}^T D B dv + D U + D \tilde{f} = 0 \quad (23)$$

For a more general material model, the function $D \tilde{s}(B D U)$ is non-linear. In the next section, it will be seen that the ALTERNAT model is not differentiable in the usual sense that can be approximated by a linear relationship.

Numerical Solution of Non-Linear Finite Element Approximation:

For non-linear problems, the solution is obtained by several iterations. It is assumed that the approximation after iteration i is Δu^i not yet satisfying Equation (20), i.e.:

$$\partial \tilde{B}^T D \tilde{s}(B D U^i) + D \tilde{f} = 1 \cdot 0 \quad (24)$$

The next iteration is in all cases derived as:

$$\mathbf{K}^i (\mathbf{D} \mathbf{U}^{i+1} - \mathbf{D} \mathbf{U}^i) = - \int_{\mathbf{v}} \dot{\mathbf{0}} \mathbf{B}^T \mathbf{D} \mathbf{S}(\mathbf{B} \mathbf{D} \mathbf{U}^i) d\mathbf{v} + \mathbf{D} \mathbf{f} \quad (25)$$

The choice of the matrix \mathbf{K}^i determines the type of iteration process. This can be best illustrated in the following non-linear equation:

$$\mathbf{g}(\mathbf{x}) = \mathbf{0} \quad (26)$$

From \mathbf{x}^i with $\mathbf{g}(\mathbf{x}^i) \neq 0$, the next approximation is obtained by:

$$\mathbf{K}^i (\mathbf{x}^{i+1} - \mathbf{x}^i) = - \mathbf{g}(\mathbf{x}^i) \quad (27)$$

This is shown graphically in Fig. (5).

The Newton-Raphson solution proceeds according to:

$$\mathbf{K}^i = \frac{d\mathbf{g}}{d\mathbf{x}}(\mathbf{x}^i) \quad (28)$$

which means that the slope of the curve for \mathbf{g} is followed:

The modified Newton-Raphson solution uses:

$$\mathbf{K}^i = \frac{d\mathbf{g}}{d\mathbf{x}}(\mathbf{x}^o) \quad (29)$$

i.e., the \mathbf{K}^i are fixed after the first one, this may be more efficient if the computation and/or the inversion of the

derivative is expensive. It is also possible to use some other $\mathbf{K}^i = \mathbf{K}$. If the \mathbf{K} is close enough to the slope of \mathbf{g} , then convergence is obtained. If the slope \mathbf{K} is steeper than the slope of \mathbf{g} , the convergence is assured, though it may be a very slow convergence.

For the case of non-linear Equations (25), the \mathbf{K}^i matrices may be defined as:

$$\mathbf{K}^i = \frac{\int_{\mathbf{v}} \mathbf{D} \mathbf{S}(\mathbf{B} \mathbf{D} \mathbf{U}^i) d\mathbf{v}}{\int_{\mathbf{v}} \mathbf{D} \mathbf{U}^i} = \mathbf{D} \mathbf{U}^i \quad (30)$$

or:

$$\mathbf{K}^i = \int_{\mathbf{v}} \dot{\mathbf{0}} \mathbf{B}^T \frac{\mathbf{D} \mathbf{S}}{\mathbf{D} \mathbf{e}} \Big|_{\mathbf{D} \mathbf{e} = \mathbf{D} \mathbf{e}^i} \quad (31)$$

This is the Newton-Raphson or tangent stiffness method in which the matrices \mathbf{K}^i are the tangent stiffness matrices.

The modified Newton-Raphson method is defined by:

$$\mathbf{K}^i = \mathbf{K} = \int_{\mathbf{v}} \dot{\mathbf{0}} \mathbf{B}^T \frac{\mathbf{D} \mathbf{S}}{\mathbf{D} \mathbf{e}} \Big|_{\mathbf{D} \mathbf{e} = \mathbf{D} \mathbf{e}^i} \quad (32)$$

Finally, the so-called initial stress method uses (Zienkiewicz, 1977):

$$K^i = K = \int_V \dot{\mathbf{B}}^T \mathbf{D} \mathbf{B} dv \quad (33)$$

where \mathbf{D} is the linearization of the elastic part of the material behaviour only.

Structure of the Finite Element Program:

The finite element program (ALTER 87) is modified from that written by Molenkamp (1987). It is based on the modified Newton-Raphson scheme. The subroutine package of Molenkamp (1987) was used together with the subroutine package of Smith and Griffiths (1988).

Description of the Problem:

Ng and Dobry (1994) made experimental tests on granular specimens of uniform spheres. The tests consist of monotonic loading on triaxial specimen and cyclic loading on simple shear specimen. The tests will be simulated using the program (ALTER 87).

Monotonic Drained Tests:

The tests were conducted on specimen B (see Table 1). The

two specimens B and C have the same size and grain size distribution and were consolidated to the same $\sigma_c = 137$ kPa. However, specimen B ($n = 0.349$) is denser than specimen C ($n = 0.382$). The ALTERNATmodel parameters for both specimens are given in Table (2). These parameters are described in the previous figures and can be seen in details in Molenkamp (1987) and Fattah (1999). The triaxial specimen was given the standard dimensions (76 mm height and 38 mm diameter) and was modelled by eight axisymmetric eight-noded isoparametric elements. The finite element mesh for the axisymmetric problem is shown in Fig. (6).

The test was conducted with constant mean stress, where the specimen was compressed in one direction and extended in other directions while the mean stress σ_m (the average of the principal stresses) is kept constant and equal to 137 kPa.

The results are presented in Fig. (7). The kinematic yield surfaces in π -plane for the initial state are shown in Fig. (8).

It is noticed in Fig. (7) that the peak stress is occurring at a very small strain (0.122). This stress-strain behaviour is attributed to the particle roundness and grain size uniformity. In Fig. (8), the outer surface is the yield surface while the interior is the plastic potential. These surfaces changes with advancement of loading.

Constant Volume Cyclic Shear Tests:

In these tests, the specimen is sheared by cycling the shear strain γ_{xy} while the volume is kept constant. By doing this, an undrained strain-controlled cyclic test similar to that typically done in many laboratories is numerically simulated.

Two specimens B and C were used to verify the influence of specimen density (porosity) on the undrained cyclic behaviour of the material.

A constant cyclic shear strain amplitude $\gamma_0 = 0.8\%$ was applied to the vertical-horizontal planes of specimen B with no volume change.

The assemblage of particles was simulated in the standard Cambridge simple shear device. The change in pore water pressure Δu is given by the relation between the apparent bulk modulus of the pore water KA and the change in volumetric strain $\Delta \epsilon_{vol}$, namely:

$$DU = KA * De_{vol} \quad (34)$$

$$KA = \frac{K_w}{n} \quad (35)$$

where: K_w = the bulk modulus of water.

Modelling the Simple Shear Device:

The dimensions of the assumed sample are 60 mm in length and 20 mm height. The finite element mesh and the boundary conditions are shown in Fig. (9). The analysis was performed in plane strain with the following boundary conditions (Dounias and Potts, 1993):

- 1) The bottom boundary was assumed rough and fully restrained.
- 2) The top boundary was assumed rigid and rough and was displaced horizontally by δ . This was achieved by tying together the nodes along the top

boundary (BC) in the x and y-directions. It was therefore free to move vertically, but it had to remain horizontal.

- 3) The vertical boundaries AB and DC were smooth and rotated in a rigid manner about their base, so that B and C were displaced horizontally by δ .

The results are presented for node 213 as shown in Figure (9).

Results of Cyclic Shear

Simulation:

In Fig. (10a), a banana-shaped stress-strain loop is developed. The curve of the shear stress versus the mean stress is shown in Fig. (10b) which shows that the mean stress during shearing is higher than the initial consolidation pressure. This implies that only negative pore pressures occur in the first two cycles. A careful study of Fig. (10b) shows that there exists an effective stress ratio line or zero-dilatancy line (shown in the figure) in both compression and extension regions, beyond which the specimen dilates.

A similar cyclic shear test was conducted on the looser

specimen C with smaller cyclic shear strain amplitude, $\gamma_0 = 0.08\%$, and the results are shown in Fig.(11).

The calculated hysteresis loops are shown in Fig.(11a) which shows a decrease of shear stress as the number of cycles increases. The shear stress decreases faster in the first cycle.

The graph of shear stress versus mean stress for this simulation, shown in Figure (11b), moves progressively towards the origin. An effective stress failure envelope can be identified both in compression and extension regions in Fig. (11b). It can be noticed that the slope of the failure envelope in compression is greater than that in extension. This means that the angle of friction in compression is greater than that in extension.

Fig. (11c) illustrates the pore pressure build-up of this simulated cyclic shear test. The plot of the calculated normalized pore pressure ratio in Fig. (11c), ($r_u = u/\sigma_c$), with number of cycles is similar to that observed in cyclic strain-controlled laboratory tests on

sands, (Finn et al., 1971 and Cho et al., 1976).

The rate of pore pressure build-up in the first cycle is the highest and decreases with number of cycles. As in the laboratory experiments, at the end of each cycle, the calculated pore pressure in Fig. (11c) increases over its value at the beginning of the cycle, and the pore pressure build-up eventually approaches the consolidation pressure where $u = \sigma_c$ or $r_u = 1$, and thus initial liquefaction occurs.

It is noticed in Fig. (11c) that the pore pressure predicted by the finite element method adopting the ALTERNAT model is less than that by the discrete element. This may be attributed to the boundary conditions adopted depending on the work of Dounias and Potts (1993) for simple shear tests. The boundary conditions make the sample more restrained and lead to smaller strains. This in turn reduces the pore pressure build-up in the sample.

Conclusions:

The finite element method is used in simulating round

uniform quartz sand under monotonic drained loading with constant mean stress and cyclic constant volume loading (undrained). The following conclusions can be drawn:

1. The peak stress is occurring at a very small strain (0.122). This stress-strain behaviour is due to the particle roundness and grain size uniformity.
2. It was found that the mean stress during shearing is higher than the initial consolidation pressure. This implies that only negative pore water pressures occur in the first two cycles. A careful study shows that there exists an effective stress ratio line or zero-dilatancy line in both compression and extension regions, beyond which the specimen dilates.
3. For cyclic simple shear test simulated in this paper, it was found that the rate of pore water pressure build-up in the first cycle is the highest and decreases with number of cycles. As in

the laboratory experiments, at the end of each cycle, the calculated pore pressure increases over its value at the beginning of the cycle, and the pore pressure build-up eventually approaches the consolidation pressure where $u = \sigma_c$ or $r_u = 1$, and thus initial liquefaction occurs.

4. It is noticed that the pore pressure predicted by the finite element method adopting the ALTERNAT model is less than that by the discrete element. This may be attributed to the boundary conditions adopted for modelling the simple shear test. The boundary conditions make the sample more restrained and lead to smaller strains. This in turn reduces the pore pressure build-up in the sample.

References:

- Bazant, Z. P. and Krizek, R. J., (1976). Endochronic Constitutive Law for Liquefaction of Sand, Journal of Engineering Mechanics, ASCE, Vol. 102, EM2, p. p. 225 - 238.
- Cho, Y., Rizzo, P.C. and Humphries, W.K., 1976. Saturated Sand and Cyclic Dynamic Tests, in "Liquefaction Problems in Geotechnical Engineering", ASCE Annual Conventional and Exposition, Philadelphia, p.p. 285-312.
- Cundal, P.A. and Strack, O.D.L., (1979). A Discrete Numerical Model for Granular Assemblies, Geotechnique, Vol. 29, No.1, p.p. 47-65.
- Dounias, G.T. and Potts, D.M., (1993). Numerical Analysis of Drained Direct and Simple Shear Tests, Journal of Geotechnical Engineering Division, ASCE, Vol. 119, GT12, p.p. 1870-1891.
- Fattah, M. Y., (1999). The Non-Linear Dynamic Behaviour of Soils, Ph.D dissertation, University of Baghdad, Iraq.
- Finn, W.D.L., Pickering, D.J. and Bransby, P.L., (1971). Sand Liquefaction in Triaxial and Simple Shear Tests, Journal of Soil

- Mechanics and Foundations Division, ASCE, Vol. 97, SM4, p.p. 639-659.
- Lade, P. V. and Duncan, J. M., (1975). Elasto-Plastic Stress - Strain Theory for Cohesionless Soil, Journal of Geotechnical Engineering Division, ASCE, Vol. 101, GT10, p. p. 1037 - 1053.
 - Molenkamp, F., (1980). Elasto-Plastic Double Hardening Model, MONOT, Report, Delft Geotechnics.
 - Molenkamp, F., (1987). Kinematic Model for Alternating Loading, ALTERNAT, Report, Delft Geotechnics.
 - Molenkamp, F., (1990). Reformulation of ALTERNAT Model to Minimize Numerical Drift Due to Cyclic Loading, Report, University of Manchester.
 - Ng, T.T. and Dobry, R., (1994). Numerical Simulation of Monotonic and Cyclic Loading of Granular Soil, Journal of Geotechnical Engineering Division, ASCE, Vol. 120, GT2, p.p. 388-403.
 - Smith, I.M. and Griffiths, D.V., (1988). Programming the Finite Element Method, Second Edition, John Wiley and Sons.
 - Zienkiewicz, O.C., (1977). The Finite Element Method, McGraw-Hill Book Company.

Table (1) – Characteristics of specimens used in simulation (from Ng and Dobry, 1994).

| Specimen | μ_s | Number and Sizes of Spheres in Specimens | | Specimen after Consolidation | | |
|----------|---------|--|---|------------------------------|--------------|-------------------------|
| | | Total Number of Particles | ($N_1/N_2/N_3$) and ($R_1/R_2/R_3$) | σ_c (kPa) | Porosity (n) | Relative Density Dr (%) |
| B | 0.5 | 398 | 291/79/28 (1/1.5/2) | 137 | 0.249 | 68.8 |
| C | 0.5 | 398 | 291/79/28 (1/1.5/2) | 137 | 0.382 | 52.0 |

Table (2) – ALTERNAT model parameters for the specimens tested by Ng and Dobry (1994) as determined by the procedure proposed by Fattah (1999).

| Parameter | Value | |
|--|------------|------------|
| | Specimen B | Specimen C |
| Non-linear Elastic Model: | | |
| V | 0.12 | 0.12 |
| A | 0.00113 | 0.00112 |
| AP | 0.327 | 0.348 |
| Deviatoric Plastic Model: Hardening or Triaxial | | |
| E | 4.19 | 4.17 |
| EP | 0.4648 | 0.4633 |
| χ_t | 0.116 | 0.122 |
| (t/s)cv | 0.655 | 0.643 |
| T | 0 | 0 |
| β | 0 | 0 |

| | | |
|---|-------------------------|-------------------------|
| χ_m | 0.049 (Molenkamp, 1987) | 0.049 (Molenkamp, 1987) |
| n_m | 5.15 (Molenkamp, 1987) | 5.15 (Molenkamp, 1987) |
| LB | 0.3 (published data) | 0.3 (published data) |
| Cohesion (c) | 0 | 0 |
| Hardening for Triaxial Extension: | | |
| EE | 1.71 | 1.69 |
| EEP | 0.2365 | 0.2314 |
| Hardening by Densification: | | |
| Porosity (n) | 0.349 | 0.382 |
| Porosity at densest state (n_{di}) | 0.27 | 0.27 |
| κ | 1 | 1 |
| Plastic Potential in pi-plane: | | |
| RT | 0.3 (published data) | 0.3 (published data) |
| Dilatancy: | | |
| ϕ_μ | 26.5° | 26.5° |
| ϕ_{cv} | 26.5° | 26.5° |
| S_{cv} | 1. | 1. |
| χ_{cv} | 1. | 1. |
| Tensile Strength: | | |
| σ_t | 0. | 0. |
| Viscosity in Liquefaction: | | |
| V_c | 0.01 sec. | 0.01 sec. |
| Initial State: | | |
| χ_i | 0.05 | 0.05 |
| Coefficient of lateral stress at rest (K_0) | 0.55 | 0.55 |

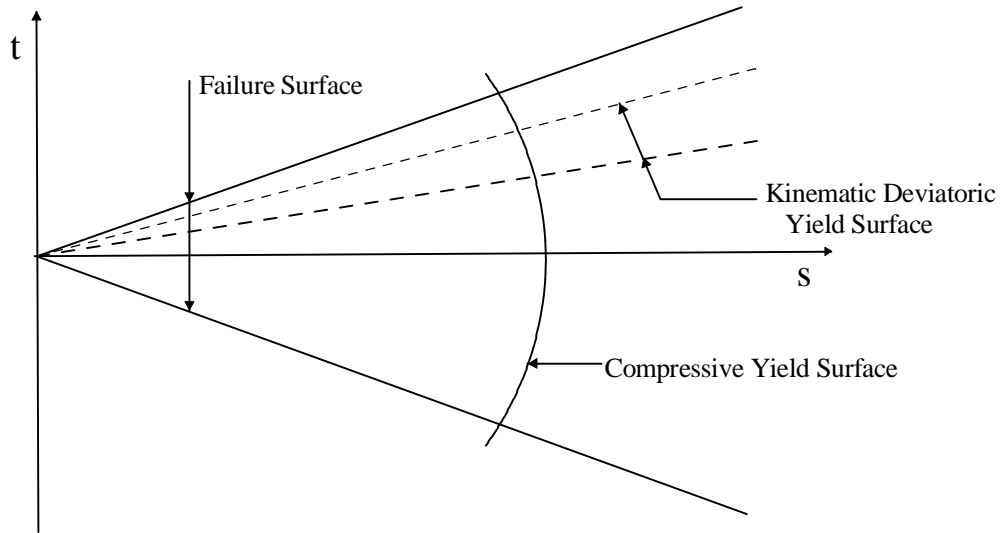
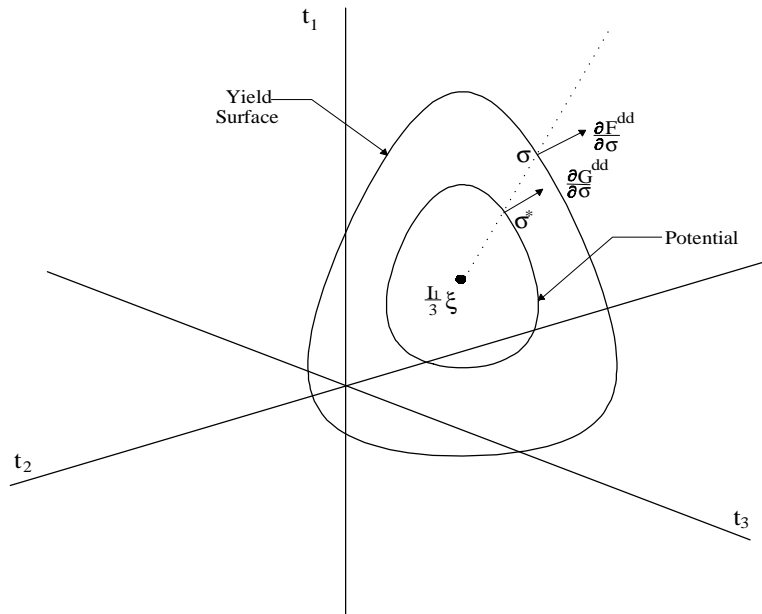


Fig. (1)- The yield surfaces of the ALTERNAT model.



Note: t_1 , t_2 and t_3 are the principal stresses.

Fig. (2)- The yield surface and the plastic potential.

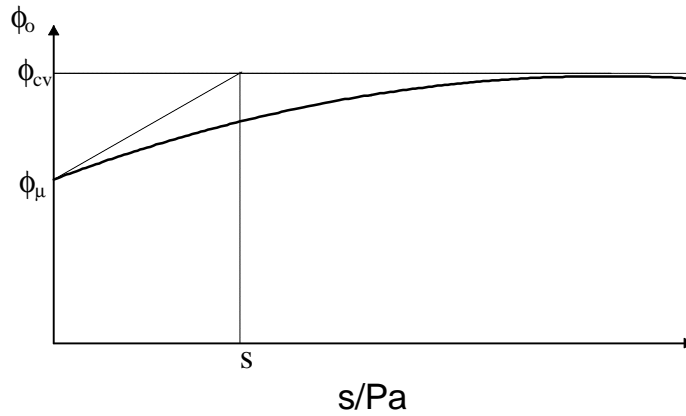


Fig. (3) – Definition of the parameters for stress dilatancy.

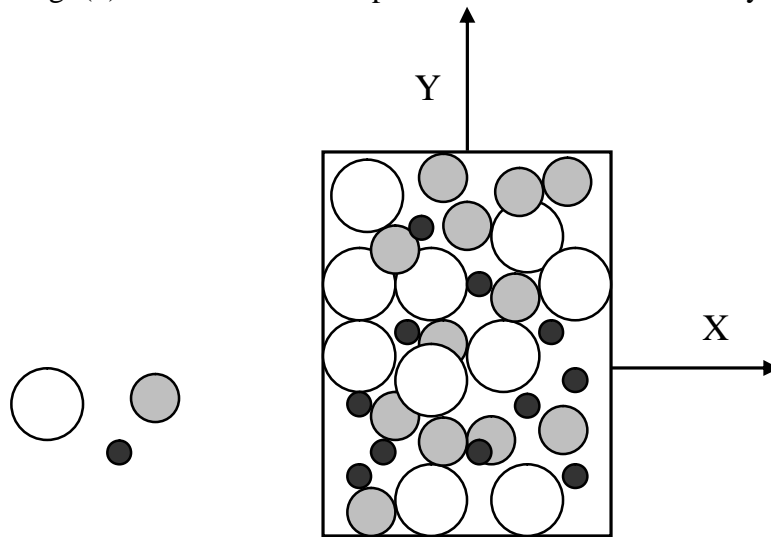


Fig. (4) – Geometry of 2-dimensional specimen used by Ng and Dobry (1994).

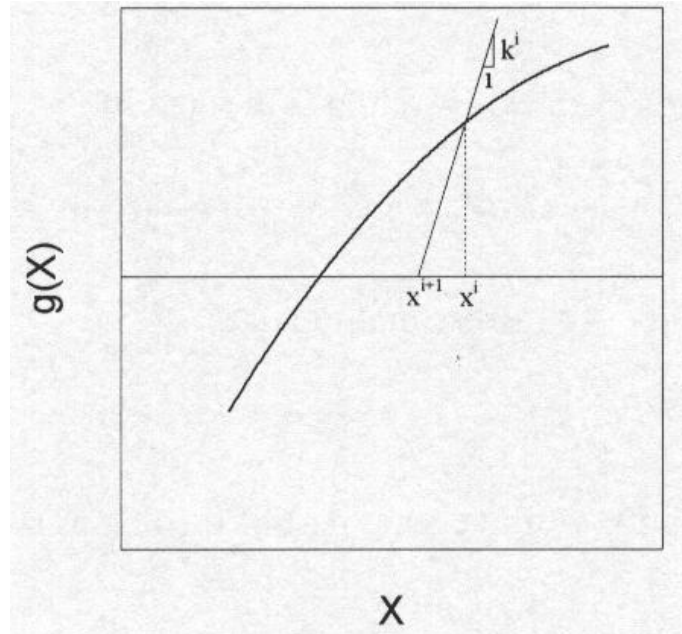


Fig. (5) – Iteration process in the non-linear problem.

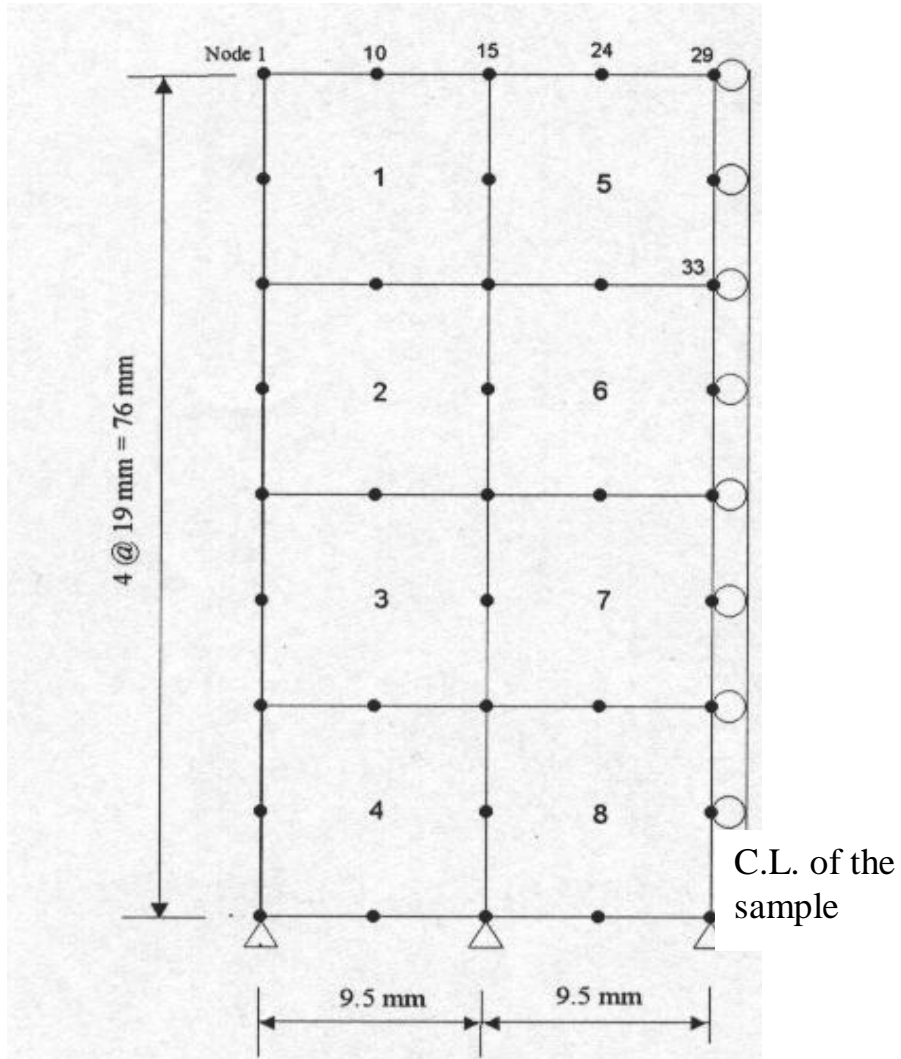


Fig.(6) – The finite element mesh for monotonic loading problem (axisymmetric).

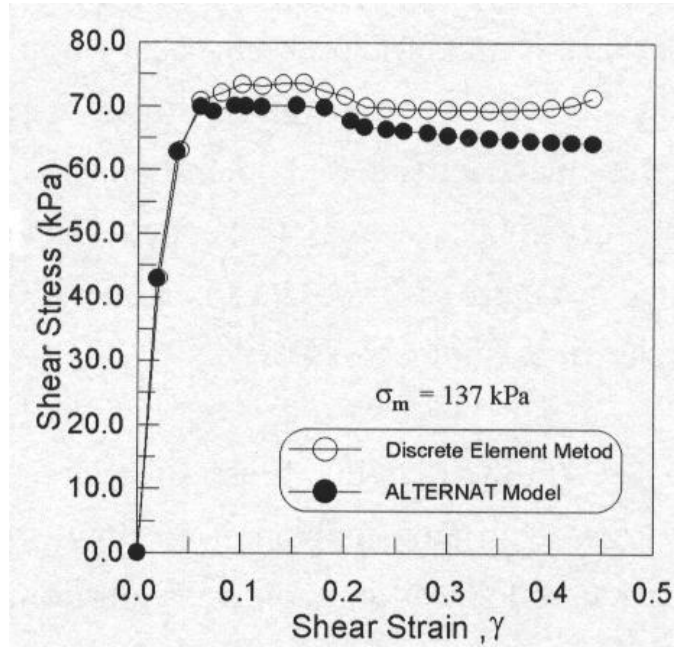


Fig. (7) – Results of drained monotonic triaxial compression test on specimen B, constant mean stress = 137 kPa.

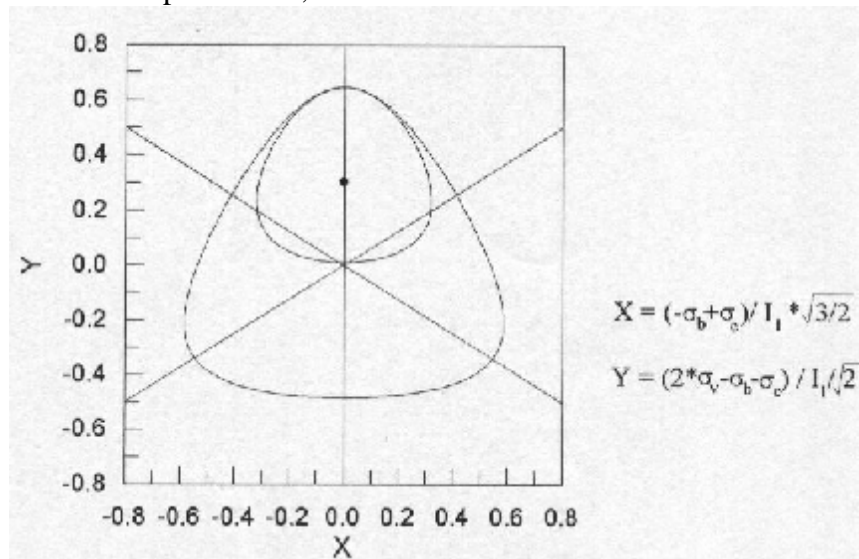


Fig. (8) – Kinematic yield surfaces in pi-plane for specimen B (initial state).

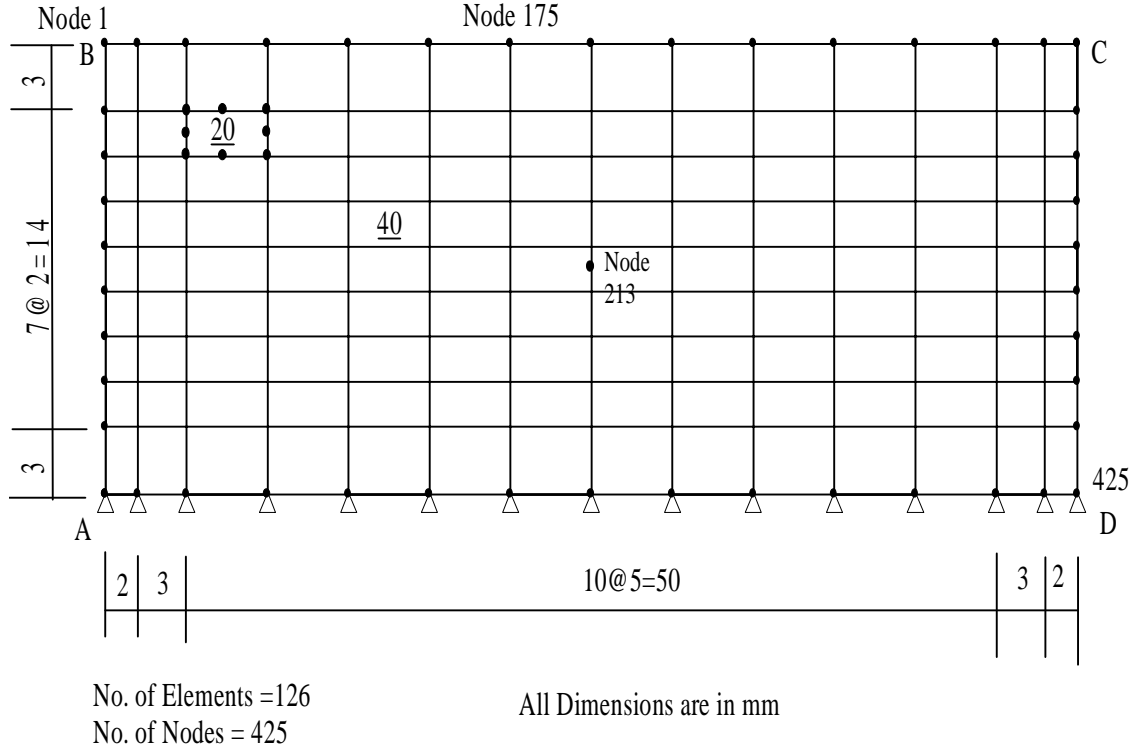
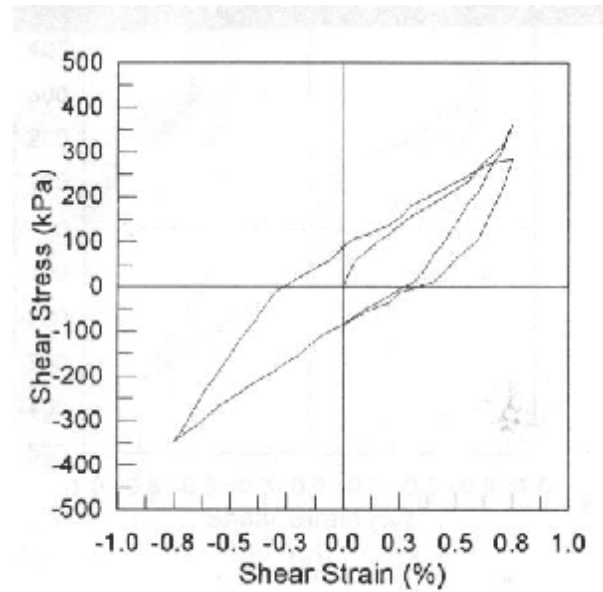
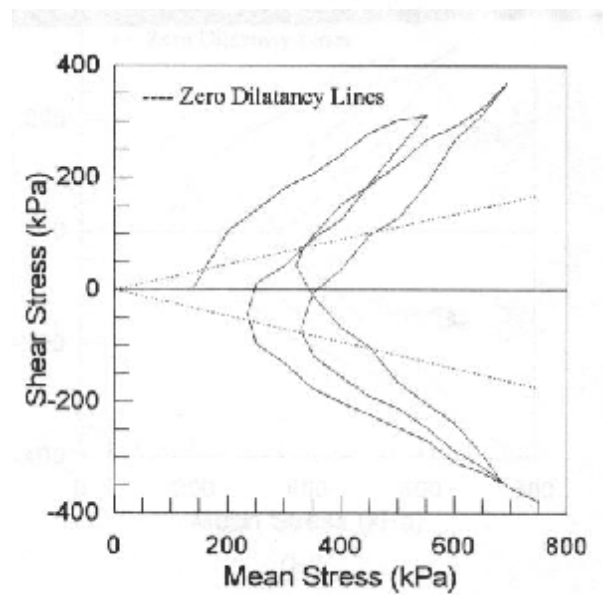


Fig. (9) – The finite element mesh and boundary conditions for simple shear analysis (plane strain).



(a)



(b)

Fig. (10) – Results of undrained cyclic shear test on specimen B.

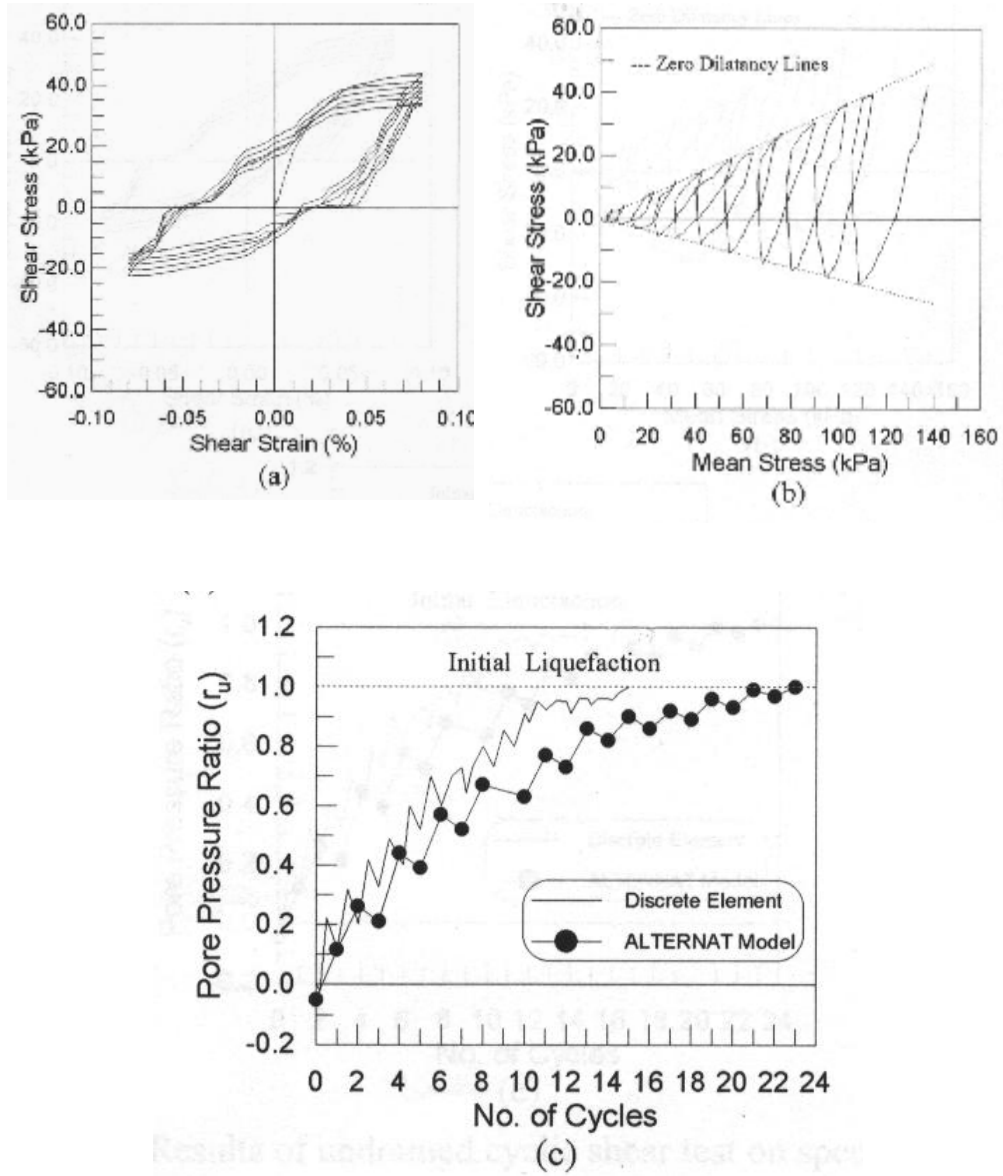


Fig. (11) – Results of undrained cyclic shear test on specimen C.